Article

Synthesis and Characterization of Quasi-Two-Coordinate Transition Metal Dithiolates M(SAr*) (M = Cr, Mn, Fe, Co, Ni, Zn; Ar* = CH-2,6(CH-2,4,6-Pr)

Tailuan Nguyen, Arunashree Panda, Marilyn M. Olmstead, Anne F. Richards, Mathias Stender, Marcin Brynda, and Philip P. Power

J. Am. Chem. Soc., **2005**, 127 (23), 8545-8552• DOI: 10.1021/ja042958q • Publication Date (Web): 17 May 2005

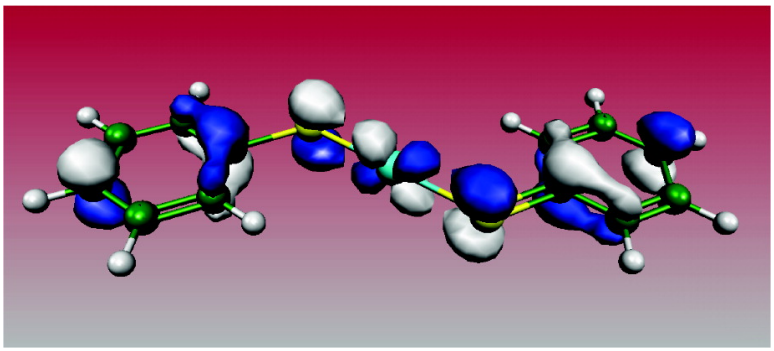

J|A|C|S
ARTICLES
Published on Web 05/17/2005

Synthesis and Characterization of Quasi-Two-Coordinate Transition Metal Dithiolates $M(SAr^*)_2$ (M = Cr, Mn, Fe, Co, Ni, Zn; $Ar^* = C_6H_3$-2,6(C_6H_2-2,4,6-Pr^i_3)$_2$

Tailuan Nguyen, Arunashree Panda, Marilyn M. Olmstead, Anne F. Richards, Mathias Stender, Marcin Brynda, and Philip P. Power*

Contribution from the Department of Chemistry, One Shields Avenue, University of California, Davis, California 95616

Received November 22, 2004; E-mail: pppower@ucdavis.edu

Abstract: A sequence of first row transition metal(II) dithiolates $M(SAr^*)_2$ (M = Cr(**1**), Mn(**2**), Fe(**3**), Co(**4**), Ni(**5**) and Zn(**6**); $Ar^* = C_6H_3$-2,6-(C_6H_2-2,4,6-Pr^i_3)$_2$) has been synthesized and characterized. Compounds **1**−**5** were obtained by the reaction of two equiv of LiSAr* with a metal dihalide, whereas **6** was obtained by treatment of $ZnMe_2$ with 2 equiv of HSAr*. They were characterized by spectroscopy, magnetic measurements, and X-ray crystallography. The dithiolates **1**, **2**, and **4**−**6** possess linear or nearly linear SMS units with further interactions between M and two ipso carbons from C_6H_2-2,4,6-Pr^i_3 rings. The iron species **3**, however, has a bent geometry, two different Fe−S distances, and an interaction between iron and one ipso carbon of a flanking ring. The secondary M−C interactions vary in strength in the sequence $Cr^{2+} \approx Fe^{2+} > Co^{2+} \approx Ni^{2+} > Mn^{2+} \approx Zn^{2+}$ such that the manganese and zinc compounds have essentially two coordination but the chromium and iron complexes are quasi four and three coordinate, respectively. The geometric distortions in the iron species **3** suggested that the structure represents the initial stage of a rearrangement into a sandwich structure involving metal-aryl ring coordination. The bent structure of **3** probably also precludes the observation of free ion magnetism of Fe^{2+} recently reported for $Fe\{C(SiMe_3)_3\}_2$. DFT calculations on the model compounds $M(SPh)_2$ (M = Cr−Ni) support the higher tendency of the iron species to distort its geometry.

Introduction

Thiolate derivatives of transition metals[1] are of great importance because of their relevance to biological metal sites in which cysteine is a ligand[2] and also because of their possible use as precursors for metal sulfides which have numerous technological applications.[3] The characterization of neutral homoleptic transition metal thiolates has, however, often encountered difficulties owing to their tendency to form insoluble polymers via thiolate bridging. This is especially true for low (two or three) coordinate transition metal complexes[4,5] where the metal is coordinatively and electronically unsaturated which increases the likelihood of association. Nonetheless, in recent years, the use of several sterically encumbered thiolate ligands[6,7] such as $-SC_6H_2$-2,4,6-Bu^t_3 (−SMes*), $-SC_6H_2$-2,4,6-Pr^i_3, $-SC_6H_3$-2,6($SiMe_3$)$_2$, $-SC_6H_2$-2,4,6-Ph_3 (STriph), and $-SC_6H_3$-2,6-Mes_2 has allowed several neutral transition metal thiolates with coordination numbers of 4 or less to be spectroscopically and structurally characterized. In particular, the ligands −SMes*[8,9] and −STriph[10] have been shown to be sufficiently bulky to stabilize essentially three-coordination in dimeric transition metal species. For the bulkier terphenyl thiolate ligand, $-SC_6H_3$-2,6-Mes_2, a monomeric, quasi-two-coordinate iron(II) derivative $Fe(SC_6H_3$-2,6-$Mes_2)_2$ can be isolated, although it has a strongly bent structure (S−Fe−S = 121.8(1)°) and displays secondary interactions between the iron and a carbon of one of the flanking mesityl rings of each terphenyl group.[11] Elsewhere, we have described the more highly encumbered ligand $-SC_6H_3$-2,6(C_6H_2-2,4,6-Pr^i_3)$_2$ (−SAr*) and its alkali metal salts.[12] The −SAr* ligand has also been used recently to stabilize the europium and ytterbium complexes $Eu(SAr^*)_2$ (S−Eu−S = 141.88(4)°) and $Yb(SAr^*)_2$ (S−Yb−S = 142.73(8)° which have strongly bent geometries as well as relatively strong (ca. 13 kcal mol^{-1}) η^6-π aromatic interactions between the metals and two of the flanking rings of the terphenyl substituents.[13] We reasoned that the very large size of this ligand might induce true two coordination at iron as well as other open shell transition metal ions in which steric effects

(1) Dance, I. G. *Polyhedron* **1986**, *5*, 1037. Krebs, B.; Henkel, G. *Angew. Chem., Int. Ed. Engl.* **1991**, *30*, 769. Kang, B.-S.; Hong, M.-C.; Wen, T.-B.; Liu, H. Q.; Lu, J.-X. *J. Cluster. Sci.* **1995**, *6*, 379. Stephan, D. W.; Nadaschi, T. T. *Coord. Chem. Rev.* **1996**, *147*, 147.
(2) See, for example, selected articles in *Chem. Rev.* **2004**, *104* (2).
(3) Lewkebandara, T. S.; Winter, C. H. *Adv. Mater*. **1994**, *6*, 237. Rees, W. S. *CVD of Non-Metals*; VCH: New York, 1996.
(4) Power, P. P. *Comments. Inorg. Chem.* **1989**, *8*, 177. Power, P. P. *Chemtracts−Inorg. Chem.* **1994**, *6*, 181.
(5) Cummins, C. C. *Prog. Inorg. Chem.* **1998**, *47*, 685.
(6) Dilworth, J. R.; Hu, J. *Adv. Inorg. Chem.* **1994**, *33*, 411.
(7) Ruhlandt-Senge, K. *Comments Inorg. Chem.* **1997**, *19*. 351.
(8) Power, P. P.; Shoner, S. C. *Angew. Chem., Int. Ed. Engl.* **1991**, *30*, 330.
(9) Rundel, R. *Chem. Ber.* **1968**, *101*, 2956.
(10) Power, P. P.; Ruhlandt-Senge, K. *Bull. Chem. Soc. Fr.* **1992**, *129*, 594.
(11) Ellison, J. J.; Ruhlandt-Senge, K.; Power, P. P. *Angew Chem., Int. Ed. Engl.* **1994**, *22*, 1178.
(12) Niemeyer, M.; Power, P. P. *Inorg. Chem.* **1996**, *35*, 7264. Niemeyer, M.; Power, P. P. *Inorg. Chem. Acta* **1997**, *263*, 201.
(13) Niemeyer, M. *Eur. J. Inorg. Chem.* **2001**, 1969.

might reduce secondary interactions with the terphenyl ligand. Two-coordinate open shell transition metal species have recently attracted interest since in certain cases they can display virtually free ion magnetism in which the orbital component makes a large, almost idealized, contribution to the magnetic moment. This was found to be the case for the strictly linear iron (II) species $Fe\{C(SiMe_3)_3\}_2$[14] where μ_B values of 6.6−7.0 were measured,[15] which is consistent with minimal orbital quenching effects of the ligand field. This effect was also supported by Mössbauer spectroscopy. We now report the synthesis and characterization of the series of metal (II) dithiolates $M(SAr^*)_2$ (M = Cr, Mn, Fe, Co, Ni and Zn). A linear or almost linear geometry is observed in all cases except for the iron compound. The $Fe(SAr^*)_2$ species displays significant bending and lengthening of one of its Fe−S bonds. The reasons for this, and its absence in the other metal dithiolates, have been explored using DFT computations.

Experimental Section

General Procedures. All work was performed by using Schlenk techniques under an atmosphere of N_2 or in a Vacuum Atmospheres HE-43 drybox. All solvents were freshly distilled from Na/K and degassed three times immediately before use. The compounds HSAr*[12] and $CrCl_2(THF)_2$[16] were synthesized by literature methods. The $FeCl_2 \cdot 4H_2O$ and $MnCl_2 \cdot 4H_2O$ complexes were purchased from commercial suppliers and dehydrated under reduced pressure in a sand bath.[17] Anhydrous $CoCl_2$ (Aldrich), anhydrous NiI_2 (Cerac), and 2.6M n-BuLi in hexanes (Acros) were purchased commercially and were used without further purification. Infrared spectra were obtained between CsI plates as Nujol mulls with use of Perkin-Elmer-1430 spectrometer. Electronic absorption spectra were obtained on a Hitachi U-2000 UV−vis spectrometer. Melting points are uncorrected and were determined for samples in capillaries sealed with grease. For magnetic measurements, the samples were sealed under N_2 in 2 mm quartz tubing. The sample magnetization was measured using a Quantum Design MPMSXL7 superconducting quantum interference device (SQUID) magnetometer. For each measurement, the sample was zero-field cooled to 5K and the magnetization was measured as a function of field to 2T. The field was then reduced to 1T, and the magnetization of the sample was measured in 5 K increments to 300 K.

$Cr(SAr^*)_2$ (1). A solution of HSAr* (1.04 g, 2 mmol) was dissolved in ca. 20 mL of diethyl ether and treated with a solution of n-BuLi (1.25 mL of a 1.6 M solution in *n*-hexane). The reaction was allowed to stir for 2 h, whereupon the solution was added to $CrCl_2(THF)_2$ (0.267 g, 1 mmol)[16] in ca. 10 mL of diethyl ether at 0 °C. The reaction was allowed to reach room temperature, and the mixture was stirred for 14 h, after which time the solvent was removed under reduced pressure. The remaining solid was dissolved with ca. 30 mL of hexane and filtered. The solution was cooled in a ca. −20 °C freezer overnight to afford the product as orange-yellow crystals. Yield: 0.507 g (47%) dec 300 °C. Anal. Calcd for $C_{72}H_{98}CrS_2$: C, 80.09; H, 9.15. Found C, 81.31: H, 9.06%. IR(Nujol, cm^{-1}): Cr−S = 370 br. UV−vis (hexane, λ_{max}, nm(ϵ, M^{-1})): 290 (200). μ_{eff}: 4.93(3)μ_B.

$Mn(SAr^*)_2$ (2). The synthesis of **2** was accomplished in a manner similar to that of **1** with use of HSAr* (1.24 g, 2.4 mmol) and $MnCl_2$ (0.15 g, 1.2 mmol). The product **2** was obtained as pale, blue-green crystals from hexane. Yield: 0.54 g (50%), M.p: dec > 252 °C. Anal. Calcd for $C_{72}H_{98}MnS_2$: C, 79.88; H, 9.12. Found C, 80.12; H, 8.98%. IR (Nujol, cm^{-1}): Mn−S = 365 m. UV−vis(hexane, λ_{max}, nm(ϵ, M^{-1})): 650 (320). μ_{eff}: 6.01(2)μ_B.

$Fe(SAr^*)_2$ (3). In a manner similar to **2,** 2.4 mmol of LiSAr* in ca. 20 mL of hexane was added to the suspension of $FeCl_2$ (0.16 g, 1.2 mmol) in ca. 10 mL of toluene via cannula of ice bath temperature. After overnight stirring at 25 °C, it was filtered and the solvent was removed under reduced pressure resulting in the formation of brick red crystals suitable for X-ray crystallographic studies. Yield: 0.85 g (79%). M.p.: 204−206 °C. Anal. Calcd for $C_{72}H_{98}FeS_2$: C, 79.81; H, 9.42. Found C, 80.23; H, 9.13%. IR (Nujol, cm^{-1}): Fe−S = 360, 410 m. UV−vis (hexane, λ_{max}, nm (ϵ, M^{-1})): 385 sh (280). μ_{eff}: 4.88-(3)μ_B.

$Co(SAr^*)_2$ (4). Compound **4** was prepared in a similar way to that described for **1** with use of HSAr* (1.04 g, 2 mmol) and $CoCl_2$ (0.13 g, 1 mmol). The product was obtained as dark, blue-green crystals. Yield: 0.570 g (53%) mp dec > 300 °C. Anal. Calcd for $C_{72}H_{98}CoS_2$: C, 79.58; H, 9.09 Found C, 79.13; H, 8.92%. IR (Nujol, cm^{-1}):Co−S, 385. UV−vis (hexane, λ_{max}, nm (ϵ, M^{-1})): 623 (185), 442 (130). μ_{eff}: 5.75(2) μ_B.

$Ni(SAr^*)_2$ (5). Compound **5** was obtained as red needles in a manner similar to that described for **1** with use of HSAr* (1.04 g, 2 mmol) and NiI_2 (0.313 g, 1 mmol). Yield: 0.532 g (49%) mp dec >300 °C. IR (Nujol, cm^{-1}) Ni−S = 390 m. UV−vis (hexane, λ_{max}, nm (ϵ, M^{-1} cm^{-1})): 864 (310), 503, (95), 450 (130). μ_{eff}: 2.58(3) μ_B.

$Zn(SAr^*)_2$ (6). A solution of $ZnMe_2$ (1 mL of a 1.0 M solution in hexane) was added dropwise via a syringe to a solution of HSAr* (1.04 g, 2 mmol) in diethyl ether (20 mL) with rapid stirring and cooling in an ice bath. The addition was accompanied by evolution of methane. Stirring was continued for 12h at room temperature, after which time the volatile materials were removed under reduced pressure. The colorless residue was redissolved in ca. 25 mL of hexane. Cooling in a ca. −20 °C freezer for 2d afforded colorless crystals of the product **6**. Yield 0.58 g (53%) mp 304−306 °C. Anal. Calcd for $C_{72}H_{98}S_2Zn$: C,79.12; H, 9.04. Found C, 79.67; H, 9.31. ^1H NMR (C_6D_6): δ 1.09 (d,*o*/*p*-CH(CH_3)$_2$), 1.31 (d,*o*/*p*-CH(CH_3)$_2$), 1.42 (d, *o*/*p*-CH(CH_3)$_2$), 2.83 (*m*,*o*-*p*-C*H*(CH_3)$_2$), 6.75−7.25 (m, aryl ^1H). ^{13}C NMR (C_6D_6): δ 24.0 (*o*-CH(CH_3)$_2$), 24.3 (*o*-CH(CH_3)$_2$), 24.8 (*p*-CH(CH_3)$_2$), 31.1 (*o*-*C*H-(CH_3)$_2$), 34.3 (*p*-*C*H(CH_3)$_2$), 120.5 (*p*-C_6H_3), 123.2 (*m*-$C_6H_2Pr^i_3$), 128.3 (*m*-C_6H_3), 138.9 (*i*-$C_6H_2Pr^i_3$), 141.2 (*o*-C_6H_3), 144.2 (*i*-C_6H_3), 146.8 (*o*-$C_6H_2Pr^i_3$), 149.9 (*p*-$C_6H_2Pr^i_3$). IR(Nujol, cm^{-1}) Zn−S = 371m.

Crystallographic Studies. Crystals of **1**−**6** were covered with a layer of hydrocarbon oil under a rapid flow of argon, mounted on a glass fiber attached to a copper pin, and placed in a N_2 cold stream on the diffractometer. X-ray data were collected on a Bruker SMART 1000 diffractometer at 90(2) K with use of MoKα radiation (λ = 0.71073 Å) (**1**, **3**−**6**) or for **2** on a Siemens P4 diffractometer at 130 K with CuKα (λ = 1.54178 Å) radiation. Absorption corrections were applied using SADABS (**1**, **3**−**6**)[18] or XABS (**2**).[19] The structures were solved with use of direct methods or the Patterson option in SHELXS[20] and refined by the full-matrix least-squares procedure in SHELXL. All non-hydrogen atoms were refined anisotropically, while hydrogens were placed at calculated positions and included in the refinement by using a riding model. Some details of the data collection and refinement are given in Table 1. Further details are in the Supporting Information.

Results and Discussion

Synthesis and Spectroscopy. The compounds **1**−**5** were synthesized in a straightforward manner, and in ca. 50−70% yield, by the addition of 2 equiv of LiSAr*, generated in situ, to the metal dihalide. Commercially available anhydrous $CoCl_2$

(14) Viefhaus, T; Schwarz, W.; Hübler, K.; Locke, K.; Weidlein, J. *Z. Anorg. Allg. Chem.* **2001**, *627*, 715. LaPointe, A. *Inorg. Chim. Acta* **2003**, *345*, 359.
(15) Reiff, W. M.; LaPointe, A.; Witten, E. H. *J. Am. Chem. Soc.* **2004**, *126*, 10206.
(16) Kern, R. J. *J. Inorg. Nucl. Chem.* **1962**, *24*, 1105.
(17) Horvath, B.; Möseler, R.; Horvath, E. G. *Z. Anorg. Allg. Chem.* **1979**, *450*, 165.
(18) *SADABS: Area-Detection Absorption Corrections*; Bruker AXS Inc.: Madison, WI, 1996.
(19) Parkin, S.; Moezzi, B.; Hope, H. *J. Appl. Crystallogr.* **1995**, *28*, 51.
(20) *SHELXS and SHELXL PC*, version 5.03; Bruker AXS Inc.: Madison, WI, 1994.

Table 1. Selected Crystallographic Data and Collection Parameters for **1**−**6**

	1	**2**	**3**	**4**	**5**·2PhMe	**6**
formula	$C_{72}H_{98}CrS_2$	$C_{72}H_{98}MnS_2$	$C_{72}H_{98}FeS_2$	$C_{72}H_{98}CoS_2$	$C_{86}H_{114}NiS_2$	$C_{76}H_{98}S_2Zn$
fw	1079.62	1082.56	1083.48	1086.55	1270.60	1092.99
color, habit	yellow, plate	dichroic blue-yellow, plate	red, plate	blue green, needle	red, needle	colorless, plate
cryst syst	triclinic	triclinic	triclinic	triclinic	monoclinic	triclinic
space group	$P\bar{1}$	$P\bar{1}$	$P\bar{1}$	$P\bar{1}$	$P2_1/c$	$P\bar{1}$
a, Å	10.380(2)	10.385(2)	10.3337(5)	11.665(3)	14.887(8)	10.212(4)
b, Å	11.535(2)	11.667(2)	11.6537(6)	16.711(3)	29.09(2)	11.282(5)
c, Å	14.359(2)	14.568(2)	14.5004(7)	18.263(4)	22.81(1)	14.540(6)
α, deg	72.834(5)	69.44(1)	70.113(1)	103.453(6)		70.942(7)
β, deg	83.944(4)	75.89(1)	75.377(1)	106.38(1)	130.73(2)	83.534(8)
γ, deg	78.820(3)	80.28(1)	80.004(1)	99.023(6)		80.246(8)
V, Å^3	1609.4(4)	1596.0(4)	1581.5(1)	3226(1)	7488(7)	1633(1)
Z	1	1	1	2	4	1
d_{calc}, Mg/m^3	1.114	1.126	1.138	1.119	1.127	1.112
θ range, deg	1.49−27.48	3.31−55.99	1.87−27.5	1.37−25.25	1.37−25.25	1.84−27.50
μ, mm^{-1}	0.282	2.574	0.344	0.370	0.358	0.478
obs data, $I > 2\sigma(I)$	5862	4158	5498	9457	6687	4012
R_1 (obs data)	0.0379	0.0358	0.0378	0.036	0.0752	0.0797
wR_2 (all data)	0.1029	0.0890	0.1058	0.1136	0.2215	0.2313

Table 2. Selected Structural Data for **1**−**6**

parameter	**1** (Cr)	**2** (Mn)	**3** (Fe)	**4** (Co)	**5** (Ni)	**6** (Zn)
M−S (Å)	2.3505(5)	2.3041(7)	2.1867(6)	2.1912(6)	2.175(2)	2.182(1)
			2.3517(6)	2.1939(5)	2.172(2)	
C(ipso)−S (Å)	1.755(2)	1.769(2)	1.767(1)	1.763(2)	1.760(5)	1.773(4)
				1.760(2)	1.764(5)	
S−M−S (Å)	180	180	151.48(2)	179.52(2)	174.22(6)	180
M−S−C(ipso) (Å)	104.87(5)	113.11(7)	128.17(5)	108.13(5)	108.2(2)	108.4(2)
			100.05(5)	108.33(5)	107.5(2)	
S−C(ipso)−C(ortho) (Å)	119.5(1)	124.72(2)	123.93(11)	122.1(1)	121.2(4)	124.5(3)
	121.4(1)	116.5(2)	117.17(10)	122.0(1)	121.9(4)	
				118.5(1)	119.1(4)	116.0(3)
				118.5(1)	118.2(4)	
M− −C(7) (Å)	2.502(2)	2.951(2)	2.427(1)	2.665(3), 2.660(3)	2.657(5), 2.640(5)	2.800(3)

afforded **4** in ca. 50% yield upon treatment with 2 equiv of the lithium thiolate. In contrast, use of commercially available anhydrous $MnCl_2$ or $FeCl_2$ did not result in good yields of **2** or **3**, and much unreacted $(LiSAr^*)_2$ was recovered from these reactions. However, employment of "activated" $MnCl_2$[17] or $FeCl_2$, which were obtained by dehydration of the tetraaquohalides $MnCl_2{\cdot}4H_2O$ or $FeCl_2{\cdot}4H_2O$ under reduced (ca. 0.01 mm Hg) pressure at ca. 150 °C, gave much smoother reactions, and up to 70% yield of the product in the case of $Fe(SAr^*)_2$. For the nickel derivative **5**, it was found that commercially available NiI_2 gave the most consistently good yields of the dithiolate. Lithium halide elimination routes were not investigated for the zinc derivative. Instead, $ZnMe_2$ (1 M in hexane) was used as the zinc source and this reacted readily with two equiv of HSAr* to afford **6** in good yield.

Magnetic studies of crystalline samples of **1**−**5** were performed in order to compare their behavior. The magnetization data were fit to a modified Curie−Weiss Law $\chi = \chi_o + C/\tau - \theta$, where C is the Curie constant and θ is the Curie temperature. The effective moment was calculated from the relationship $\mu_{eff} = (8C)^{1/2}$. The μ_B values for **1**−**5** indicate that they are all high-spin consistent with 4, 5, 4, 3, and 2 unpaired electrons, respectively. Plots of $1/\chi$ versus temperature displayed a linear relationship in the range of 5−300 K. IR spectra of **1**−**6** displayed a medium intensity, broad absorption in the range of 350−390 cm^{-1} assignable to an M−S vibration that corresponds to the asymmetric stretching of the linear or quasi linear MS_2 unit. The UV−visible spectra of **1**−**5** are characterized by intense broad absorptions in the UV region that extend into visible wavelengths and can be attributed to thiolate sulfur to metal change transfer phenomena. Although weak shoulder features could be observed in the spectra of **1** and **3**, well-defined d−d transitions at longer wavelengths than the change transfer "front" could only be observed in the spectra of **4** and **5**.

Structures. Selected structural data for **1**−**6** are provided in Table 2. The structures of **1**−**6** are exemplified by the thermal ellipsoid plots given in Figures 1−3.

With the exception of the iron thiolate **3**, where the S−Fe−S angle is 151.48(2)°, the compounds are characterized by a linear, or almost linear, S−M−S arrangement at the metal. In addition, the ipso carbons of the central aryl rings of the terphenyl groups form an almost coplanar array with the SMS unit. For example, the CSMSC array is exactly planar in **1**, **2**, **3**, and **6**, where the angle between the two MSC planes is 0°, whereas the angle is only 1.5° for **4** although it is a somewhat larger 15.9° for **5**. With the exception of **5**, the CSMSC core planarity almost extends to the central aryl ring planes of the terphenyl ligands where relatively small interplanar angles of 4.0°(Cr), 8.2°(Mn), 10.8°(Fe), 1.1°(Co), 5.7°(Ni), and 2.1°(Zn) observed between the MSC and aryl ring planes.

The M−S distances decrease from ca. 2.35 to 2.17 Å across the open shell series **1**−**5** with a slight increase being observed (to ca. 2.18 Å) for the d^{10} compound **6**. The S−C(ipso) distances fall in the narrow range 1.755(2) to 1.773(4) Å. The M−S−C(ipso) angles show greater variation and are narrowest at chromium (104.87(5)°) and in the distorted iron species **3**

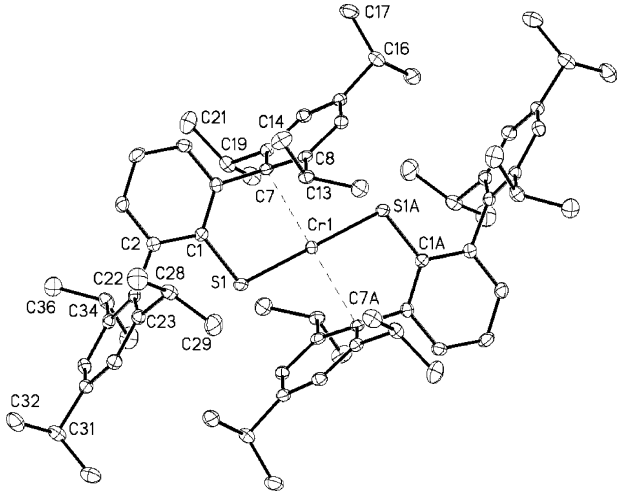

Figure 1. Thermal ellipsoid plot (30%) of $Cr(SAr^*)_2$, **1**, showing the linear S−Cr−S coordination and Cr− −C(ipso) interactions. Hydrogen atoms are not shown. Selected distances and angles are given in Table 2.

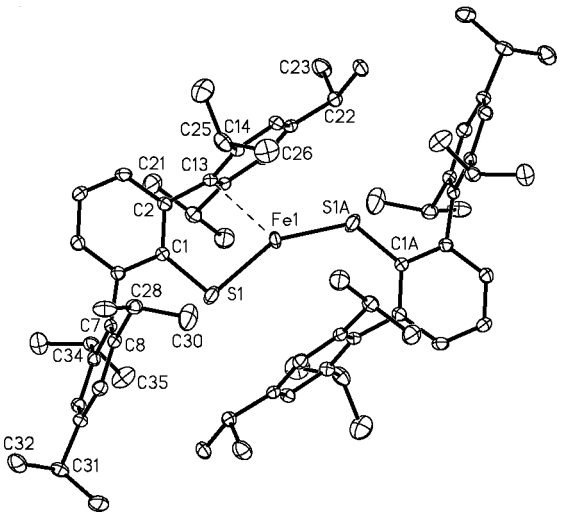

Figure 2. Thermal ellipsoid plot (30%) of $Fe(SAr^*)_2$, **3**, showing the bent S−Fe−S arrangement and interaction between Fe and C(13) of the S(1)-Ar* ligand. Hydrogen atoms are not shown. Selected distances and angles are in Table 2.

(100.03(4°)). There are only small differences between the S−C(ipso)C(ortho) angles at the central ring of the terphenyl ligands (Table 2). All compounds display relatively close approaches (<3.0 Å) between ipso carbon(s) of one of the flanking C_6H_2-2,4,6-Pr^i_3 rings of the terphenyl group and the metal centers. These distances are listed in Table 2 and vary from 2.427(1) in **3** to 2.951(2) Å in the manganese compound **2**. Because of the symmetry, the structures of $MS_2(Cipso)_2$ units for **1**−**4** and **6** form an approximate square planar array. There is also a noticeable distortion of the geometry at the ipso carbon of the ring that interacts with the metal. This distortion is observable in Figures 1−3, and it can be expressed in terms of the angle between the connecting C(6)−C(7) carbon−carbon bond and the plane of the interacting aryl ring. For **1**−**6**, this angle has the values **1**(25.1°), **2**(5.6°), **3**(5.7°), **4**(10.3°), **5**(20.3°) and **6**(14.6°).

The structure of the iron compound **3** differs from those of **1**, **2** and **4**-**6** in the extent of the bending of the metal geometry, S−Fe−S = 151.48(2)°. The iron is disordered over two positions, each of which has 50% occupancy. This results in

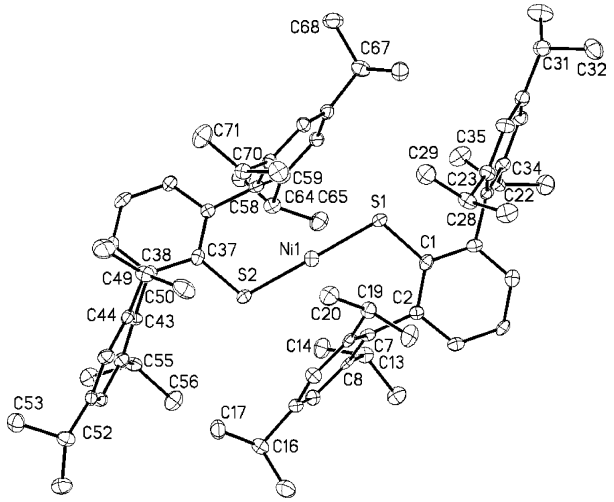

Figure 3. Thermal ellipsoid plot of $Ni(SAr^*)_2$, **5**, showing the slightly bent S−Ni−S unit. Hydrogen atoms are not shown. Selected distances and angles are given in Table 2.

two quite different (by ca. 0.16 Å) Fe−S bond lengths and Fe−S−C(ipso) angles that differ by ca. 28°. The narrower angle is associated with the longer Fe−S distance and the terphenyl group that more closely approaches the iron center. The possible origins of the different structure of the iron species will be discussed below.

Discussion

The compounds **1**−**5** are quite rare examples of formally two-coordinate open shell (d^1−d^9) transition metal complexes.[4] They are also notable because, with the exception of the iron compound **3**, their S−M−S geometries are linear or close to linear. This is in contrast to geometries of some other formally two coordinate transition metal species, especially those of Cr^{2+},[21,22] Co^{2+},[22,23] and Ni^{2+},[21,22] where only nonlinear metal coordinations are currently known. The thiolates **1**-**6** are precedented only by $Fe(SC_6H_3$-2,6-$Mes_2)_2$[11] (Mes = C_6H_3-2,4,6-Me_3; S−Fe−S = 121.8(1)°; Fe−S = 2.276(2) Å; Fe−C = 2.470(3), 2.535(3) Å) and $Zn\{SC_6H_3$-2,6-$Mes_2)_2$[24] (S−Zn−S = 151.7(1)°; Zn−S = 2.192(2) Å; Zn−C = 2.651(2), 2.718(2) Å} which are the only structurally characterized neutral, divalent, homoleptic transition metal, or zinc thiolate monomers previously known. These compounds employ the related, less sterically crowding ligand $-SC_6H_3$-2,6-Mes_2 and they display much greater bending at their metal geometries than **3** or **6**. In general, there are relatively few structurally characterized neutral homoleptic thiolate complexes for many mid to late transition metal ions except those of groups 10 and 11. For instance, in the case of Cr(II) no structural data for such compounds are currently available and structural data for any type Cr(II) complex with a terminal thiolate ligand are quite scarce.[25] A recent example is the complex (η^5-C_5H_5)$(CO)_2CrSN_2C_4H_3$ ($SN_2C_4H_3$ = 2-thiolatopyrimidine)[26] where the observed Cr−S

(21) Bartlett, R. A.; Chen, H.; Power, P. P. *Angew. Chem., Int. Ed. Engl.* **1989**, *28*, 316.
(22) Chen, H.; Bartlett, R. A.; Olmstead, M. M.; Power, P. P.; Shoner, S. C. *J. Am. Chem. Soc.* **1990**, *112*, 1048.
(23) Bartlett, R. A.; Power, P. P. *J. Am. Chem. Soc.* **1987**, *109*, 7563.
(24) Ellison, J. J.; Power, P. P. *Inorg. Chem.* **1994**, *33*, 4231.
(25) Danopoulos, A. A.; Wilkinson, G.; Sweet, T. K. N.; Hursthouse, M. B. *Dalton Trans.* **1995**, 2111.
(26) Ng, V. W. L.; Leong, W. K.; Koh, L. L.; Tan, G. K.; Goh, L. Y. *J. Organomet. Chem.* **2004**, *689*, 3210.

distance is 2.449(2) Å. This is ca. 0.1 Å longer than that observed in **1**. The difference may be attributed in part to the higher effective coordination number (7) of the $(\eta^5\text{-}C_5H_5)(CO)_2\text{-}CrSN_2C_4H_3$ species.

A greater number of Mn(II) thiolates have been characterized, but most of these involve manganese coordination numbers of four or higher in negatively charged complexes.[27] There exist only two neutral manganese complexes with terminal thiolate ligands in which the formal metal coordination number is less than four. These are the thiolate bridged dimers $\{Mn(SMes^*)_2\}_2$[8] ($Mes^* = C_6H_2\text{-}2,4,6\text{-}Bu^t_3$) and $\{Mn(SAr)_2\}_2\cdot THF$[28] ($Ar = C_6H_3\text{-}2,6\text{-}(SiMe_3)_2$) which have similar thiolate bridged structures except that in the latter species one of the manganese atoms is also coordinated to THF. In $\{Mn(SMes^*)_2\}_2$ the terminal Mn−S bond length is 2.317(3) Å[8] and the Mn−S distance to three coordinate manganese in $\{Mn(SAr)_2\}\cdot THF = 2.343(1)$ Å.[28] The 2.3041(7) Å Mn−S bond length observed in **2** is thus marginally shorter than either of these, which in agreement with the lower coordination number of the metal and despite the larger size of the −SAr* ligand.

In contrast to their Cr(II) and Mn(II) analogues, Fe(II) thiolates are the most studied transition metal thiolates because of the widespread presence of iron−sulfur coordination in a variety of metallobiomolecules.[29] Numerous examples have been structurally characterized. However, the most relevant structures comparable to **3** are confined to a handful of compounds, which includes the already mentioned $Fe(SC_6H_3\text{-}2,6\text{-}Mes_2)_2$(Fe−S(tml) = 2.276(2) Å),[11] { $Fe(SC_6H_2\text{-}2,4,6\text{-}Ph_3)_2\}_2$ (Fe−S(tml) = 2.262-(3) Å), Mes*SFe(μ-SMes*)$_2$Li(THF)$_2$,(Fe−S(tml) = 2.259(4) Å),[30] $[PPh_4]$ $[Fe(SMes^*)_3]\cdot 2MeCN\cdot C_7H_8$ (Fe−S avg = 2.27-(1) Å[30] and $\{Fe(SMes^*)_2\}_2$(Fe−S(tml) = 2.256(3) Å).[8] Thus, the Fe−S distances in these nominally three coordinate complexes fall within the remarkably narrow range 2.256(3) to 2.276(2) Å. Most notably, the average of the two Fe−S distances in **3** (2.269 Å) is also within these limits. The absence of shortening in the average Fe−S distance in **3** is consistent with the distortion in the structure due to the strong Fe−C interaction which increases the effective coordination number of iron from two to three.

Several anionic thiolate derivatives of cobalt(II) are known.[31] However, the most relevant previously published cobalt (II) thiolate structure to **4** concerns the dimer $\{Co(SMes^*)_2\}_2$[8] which is isostructural to its iron and manganese analogues discussed above. It has a formally three coordinate cobalt and a terminal Co−S distance of 2.222(2) Å. The average Co−S distance in **4**, 2.1925(13) Å, is slightly shorter than this, but it is within 3σ of 2.222(2) Å. The absence of a significant Co−S bond contraction is consistent with two Co− -C interactions (discussed below) which increase the effective coordination number.

There have been several structural reports for neutral nickel-(II) thiolates but, without exception, these involve aggregated species of formula $\{Ni(SR)_2\}_n$ ($n = 4,5,6,8$),[32] in which nickel is four-coordinate and the thiolates bridge the metals. In these compounds Ni−S distances near 2.20 Å are usually observed. The Ni−S average bond length in **5** of 2.174(12) Å is somewhat shorter and is in accordance with the lower formal coordination number of the metal. However, the small amount of shortening observed in **5** (ca. 0.025 Å) suggests that the short Ni−C interactions, and the higher effective coordination number (see below) may play a role in maintaining a longer Ni−S distance. The 2.182(1) Å Zn−S distance in **6** is marginally, but significantly shorter than the 2.193(1) and 2.199(1) Å distances seen in $Zn(SC_6H_3\text{-}2,6\text{-}Mes_2)_2$.[24] However, the geometry of Zn-$(SC_6H_3\text{-}2,6\text{-}Mes_2)_2$ is bent and there are short Zn−C contacts of 2.651(2) and 2.718(2) Å (cf 2.800(3) Å in **6**) that increase the effective coordination number of Zn and so increase the Zn−S bond distances in comparison with those in **6**. The Zn−S bond length in $(Et_2O)Zn(SMes^*)_2$ (Zn−S = 2.196(3) Å)[33] and the terminal Zn−S bond in the dimer $\{Zn(SMes^*)_2\}_2$ (2.193-(3) Å),[34] both of which feature three coordinate zinc, are also longer than that in **6**.

The structures of **1**−**6** are also characterized by M−C interactions of various strengths with one (**3**) or two ipso carbons (**1**, **2**, **4**−**6**) of a flanking $-C_6H_2\text{-}2,4,6\text{-}Pr^i_3$ ring(s) of the terphenyl ligands. These interactions resemble those reported earlier for $Fe(SC_6H_3\text{-}2,6\text{-}Mes_2)_2$ or $Zn(SC_6H_3\text{-}2,6\text{-}Mes_2)_2$. The similarity of the M−C distances in these complexes and those in **3** and **6**, together with the very different bending angles observed in the two sets of compounds, suggest that the linear geometry in **1**−**6** is dictated by the size of the ligand. All the M−C contacts in these compounds and **1**−**6** are significantly longer than single M−C bonds. For instance, the Fe−C single bond lengths in $MnMes^*_2$,[35] $FeMes^*_2$,[35,36] and $ZnMes_2$[37] are 2.108(2), 2.058(4), and 1.942(2) Å respectively. Thus, for the Mn and Zn thiolates **2** and **6** the M−C distances are ca. 0.85 Å longer than those expected for single M−C bonds. For the Fe−C distances, however, the difference is much less (ca. 0.37 Å). It may also be noted that the M−C distances are shorter in the iron complex (giving presumably a much stronger M−C interaction) than in any of its transition metal or zinc congeners. Inspection of the structural data for **1**−**6** indicate that the only M−C interactions of comparable strength to those in the iron species are those of the chromium thiolate **1**. Bearing in mind that Cr^{2+} has a slightly larger effective ionic radius than Fe^{2+} (0.80 vs 0.78 Å),[38] it can be generalized that the strength of the M−C interactions in **1**−**6** follow the sequence Cr ≈ Fe > Co ≈ Ni > Mn > Zn. Crystal field factors could play a role in the M−C interactions. However, with the exception of the d^5 complex **2** where such a factor is absent, the magnitude of the M−C interactions reflect the electron deficiency of the metal centers. Thus, in the case of **1**, where M−C interactions are

(27) Costa, T.; Dorfman, J. R.; Hagen, K. S.; Holm, R. H. *Inorg. Chem.* **1983**, *22*, 4091.
(28) Stephan, H.-O.; Henkel, G. *Inorg. Chem. Acta* **1994**, *219*, 1.
(29) Cammack, R. *Adv. Inorg. Chem.* **1992**, *38*, 281. Block, E.; Zubieta, J. *Adv. Sulfur. Chem.* **1994**, *1*, 133. Stillman, M. J. *Coord. Chem. Rev.* **1995**, *144*, 461.
(30) MacDonnell, F. M.; Ruhlandt-Senge, K.; Ellison, J. J.; Holm, R. H.; Power, P. P. *Inorg. Chem.* **1995**, *34*, 1815.
(31) Dance, I. G.; Calabrese, J. C. *Chem. Commun.* **1975**, 762.
(32) For example: Woodward, P.; Dahl, L. F.; Abel, E. W. *J. Am. Chem. Soc.* **1965**, *87*, 5251. Gould, R. O.; Harding, M. M. *J. Chem. Soc. A* **1970**, 875. German, C.; Declerq, J. P. *Polyhedron* **1984**, *3*, 969. Gaebe, W.; Ros, T.; Solons, X.; Font-Atlaba, M.; Brianso, J. L. *Inorg. Chem.* **1984**, *23*, 39. Dance, I. G.; Scudder, M. L.; Secomb, R. *Inorg. Chem.* ***1985***, *24*, 1201. Feld, H.; Leute, A.; Rading, D.; Benninghoven, A.; Henkel, G.; Krüger, T.; Krebs, B. *Z. Nat.* **1992**, *47*, 929. Mahmeredkhani, A. H.; Langer, V. *Polyhedron* **1999**, *18*, 3407 and references therein.
(33) Power, P. P.; Shoner, S. C. *Angew Chem. Int. Ed.* **1990**, *29*, 1403.
(34) Bochmann, M.; Bwemba, G.; Grinter, R.; Lu, J.; Webb, K. J.; Williamson, D. J.; Hursthouse, M. B.; Mazid, M. *Inorg. Chem.* **1993**, *32*, 532.
(35) Wehmschulte, R. J.; Power, P. P. *Organometallics* **1995**, *14*, 3264.
(36) Müller, H.; Seidel, W.; Görls, M. *Angew. Chem., Int. Ed. Engl.* **1995**, *36*, 325.
(37) Cole, S. C.; Coles, M. P.; Hitchcock, P. B. *Dalton Trans.* **2003**, 3663.
(38) Shannon, R. D. *Acta Crystallogr.* **1976**, *A32*, 751.

Scheme 1. Drawing of the Possible Structural Rearrangement of the Model Iron Dithiolate $Fe(SPh)_2$

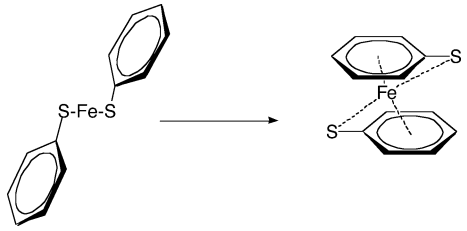

among the strongest, the formal valence electron count is 8, whereas in **6**, where the M−C interaction is weakest, it is 14.

Do the short metal carbon interactions induce structural deformities other than changing the angle between the vector that connects the interacting $-C_6H_2$-2,4,6-Pr^i_3 ring to the central aryl ring as mentioned in the structural description? Examination of the bond distances and angles show that the C−C interactions bond adjacent to the ipso carbon of the interacting flanking aryl ring is not lengthened in comparison to the C−C bond that connects the noninteracting flanking ring in the same ligand. For instance in **5** the C(6)−C(7) (1.508(7) Å) and C(6)−C(22) (1.519(6) Å) distances are within 1.5 standard deviations of each other. Similarly, examination of the average C(ipso)−C(ortho) distances within the interacting and noninteracting aryl rings shows that the differences in bond lengths are not statistically significant. Mössbauer[30,39] studies of low coordinate iron(II) thiolates show that the observed Fe−C approaches are short enough to distort the electron density of the metal and cause different isomer shifts thus supporting an increased coordination number.[39] However, the Fe−C approaches do not appear to be strong enough to cause significant lengthening of the C−C bonds in the interacting ligands. Thus the interactions are of a secondary type probably involving energies of ca. 5−10 kcal mol^{-1} which can distort the relatively soft S−M−S angles at the metal. Nonetheless, it is probable that the M−C interactions in the linear or near linear compounds **1**, **4**, and **5** are sufficient to essentially quench orbital contributions to the magnetic moment. The magnetic data for these are near to spin only values and do not provide any evidence of the "free ion" magnetism recently reported for $Fe[C(SiMe_3)_3]_2$.[15] It is believed that this phenomenon is associated with the strictly linear two-coordinate structure of this compound where the closest secondary metal−ligand interactions involve hydrogens from the $-C(SiMe_3)_3$ ligand that distances are in the range 2.83−3.04 Å. These are significantly longer and weaker than the M−C interactions in **1**, **4**, and **5** and are apparently too weak to affect the magnetic properties of the complex. Large angular momentum contributions to the magnetic moment have also been noted for three-coordinate iron β-diketiminate complexes.[40]

The general trends in the M−C interactions and their effects discussed above do not account for the type of structural distortion found in the iron compound **3**. At present, we hypothesize that the distortion represents the initial stage of a structural rearrangement to form a sandwich species involving an aryl rings from the terphenyl ligands. This may be illustrated (Scheme 1) for the simple model species $Fe(SPh)_2$.

The possibility of such a rearrangement is supported by previous studies on molybdenum (III) thiolate derivatives and

Scheme 2. Schematic Drawing of $Mo(\eta^6$-C_6H_3-2,6$(SiMe_3)_2)(\eta^7$-C_6H_3-2,6$(SiMe_3)_2)$[43]

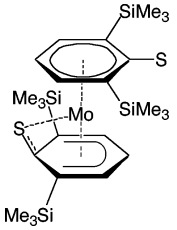

DFT calculations.[41] For the molybdenum compounds, the use of the thiolate $-SC_6H_2$-2,6-Mes_2 afforded $Mo(SC_6H_3$-2,6-$Mes_2)_3$,[42] which displayed very strong η^6 interactions with one of the phenyl rings of the terphenyl group. However, with use of the thiolate $-SC_6H_3$-2,6-$(SiMe_3)_2$ a diamagnetic Mo(II) derivative was obtained[43] which has the illustrated sandwich structure (Scheme 2) with η^6 and η^7 bound aryl thiolate ligands. DFT calculations were performed on **1**−**6** using hybrid B3LYP functional in conjunction with ECP LanL2DZ and 6−31G* basis sets.[41] For the geometry optimizations, simplified $M(SPh)_2$ models (where the bulky terphenyl substituents were replaced by phenyl rings) were used. Two sets of starting geometries were considered: one in which all the atoms were coplanar and the other in which the phenyl rings were rotated at 90° to the plane containing the C(ipso)−S−M−S−C(ipso) fragment. In this case, the optimized structure of the model compound containing the iron atom clearly showed a "sandwich" type conformation (sketched above), where the iron lies mid-way between two phenyl rings. The sandwich structure is 9.9 kcal $mole^{-1}$ more stable than the undistorted planar PhSFeSPh structure (Scheme 1) at the B3LYP/LanL2DZ level. In contrast, the calculated energy differences for the two model structures featuring Cr, Mn, Co or Ni displayed much smaller (ca. 2−3 kcal mol^{-1}) energy differences between the structures in which

(39) Evans, D. J.; Hughes, D. L.; Silver, J. *Inorg. Chem.* **1997**, *36*, 747.
(40) Andres, H. P.; Bominaar, E. L.; Smith, J. M.; Eckert, N. A.; Holland, P. L.; Münck, E. *J. Am. Chem. Soc.* **2002**, *124*, 2002.

(41) The geometry optimizations of the model $M(SPh)_2$ compounds were performed in the gaseous phase using DFT theory with hybrid B3LYP functional. The molecular structures of two types were considered: The in-plane (IP) structures with the phenyl rings coplanar with the C−S−Me−S−C fragment and (OP) out-of-plane structures where the phenyl rings make 90 degrees with the plane containing C−S−Me−S−C fragment. Both type of structures were optimized with Los Alamos LanL2DZ basis set using an effective core potential (ECP) approximation; a subsequent optimization of the geometry was performed with 6−31 g* basis set using unrestricted calculations for low spin (LS) and high spin (HS) complexes, except for Zn complex, where restricted calculations were performed. Adiabatic LS/HS energy differences were calculated by comparing energies obtained from the LS and HS optimized geometries. All the calculations were performed with the Gaussian 03 package[a], and the representations of the molecular structures and molecular orbitals were generated with the MOLEKEL program[b]. (a) Frisch, M. J.; Trucks, G. W.; Schlegel, H. B.; Scuseria, G. E.; Robb, M. A.; Cheeseman, J. R.; Montgomery, J. A.; Vreven, T., Jr.; Kudin, K. N.; Burant, J. C.; Millam, J. M.; Iyengar, S. S.; Tomasi, J.; Barone, V.; Mennucci, B.; Cossi, M.; Scalmani, G.; Rega, N.; Petersson, G. A.; Nakatsuji, H.; Hada, M.; Ehara, M.; Toyata, K.; Fukuda, R.; Hasegawa, J.; Ishida, M.; Nakajima, T.; Honda, Y.; Kitao, O.; Nakai, H.; Klene. M.; Li, X.; Knox, J. E.; Hratchian, H. P.; Cross, J. B.; Adamo, C.; Jaramillo, J.; Gomperts, R.; Stratmann, R. E.; Yazyev, O.; Austin, A. J.; Cammi, R.; Pomelli, C.; Ochterski, J. W.; Ayala, P. Y.; Morokuma, K.; Voth, G. A.; Salvador, P.; Dannenberg, J. J.; Zakrzewski, V. G.; Dapprich, S.; Daniels, A. D.; Strain, M. C.; Farkas, O.; Malick, D. K.; Rabuck, A. D.; Raghavachari, K.; Foresman, J. B.; Ortiz, J. V.; Cui, Q.; Baboul, A. G.; Clifford, S.; Ciolowski, J.; Stefanov, B. B.; Liu, G.; Liashenko, A.; Piskorz, P.; Komaromi, I.; Martin, R. L.; Fox, D. J.; Keith, T.; Al-Laham, M. A.; Peng, C. Y.; Nanayakkara, A.; Challacombe, M.; Gill, P. M. W.; Johnson, B.; Chen, W.; Wong, M. W.; Gonzalez, C.; Pople, J. A. *Gaussian 03*, Revision A.1; Gaussian, Inc.: Pittsburgh, PA, 2003. (b) Flukiger, P.; Luthi, H. P.; Portmann, S.; Weber, J. *MOLEKEL 4.3*; Swiss Center for Scientific Computing: Manno, Switzerland, 2000−2002.
(42) Buyuktas, B. S.; Olmstead, M. M.; Power, P. P. *Chem. Commun.* **1998**, 1689.
(43) Komuro, T.; Matsuo, T.; Kawaguchi, H.; Tatsumi, K. *J. Am. Chem. Soc.* **2003**, *125*, 2070.

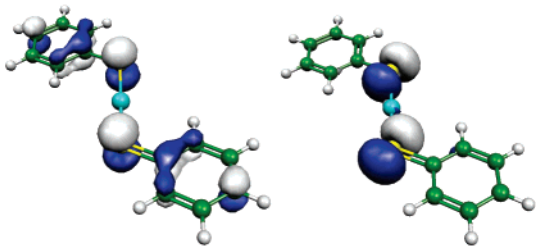

Figure 4. The π_{op} and π_{ip} molecular Kohn−Sham orbitals of the thiolate ligands.

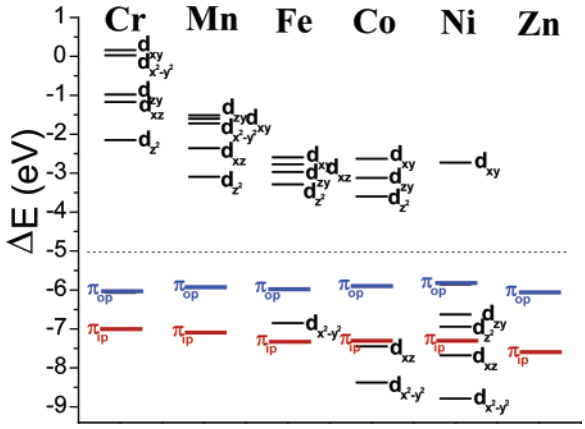

Figure 5. Energy diagram for the relevant spin-down Kohn−Sham orbitals obtained from the unrestricted DFT calculations on the high-spin transition metal thiolate complexes $M(SPh)_2$. Restricted calculations were used for Zn complex.

the phenyl rings were coplanar and at 90° to the SMS units and there were no distortions from linear geometries.

The calculated DFT geometries of the model $M(SPh)_2$ species were also used to provide insight into the bonding scheme in the dithiolate complexes. Using a similar notation to the known thiolate-transition metal systems[44] the molecular orbitals of the ligands were labeled as π_{op} (out-of-plane) or π_{ip} (in-plane) (Figure 4). From the unrestricted open-shell calculations, the relevant spin-down orbitals were used to analyze the bonding scheme, since the metal−thiolate bonding is associated with the allowed transitions from the occupied thiolate-based spin down levels into empty metal atom-like spin down 3d orbitals. For the Zn complex **6**, doubly filled MO's from spin-restricted calculations were analyzed. In all the model complexes, except that of Zn, the lowest energy is associated with the π_{ip}, while the π_{op} is in all cases the HOMO orbital.

The ground-state energies for the relevant MO's are reported in Figure 5. As can be seen from the MO energy diagram, the metal spin down 3d orbitals decrease in energy relative to the thiolate MO's when proceeding from left to the right across the row. This is mainly due to the relative nuclear charge of the metal atoms. The highest energy gap between the thiolate π_{op} and the empty LUMO d orbital is observed the in Cr model complex. The gap diminishes to the Fe model complex where a reversal in the d orbital order is observed. The $d_{x^2-y^2}$ orbital lies between the π_{ip} and the π_{op} thiolate MO's. This situation is even more pronounced for the remaining model complexes of the series: In the Co complex the model d_{xz}, and $d_{x^2-y^2}$ orbitals

(44) Fox, D. C.; Fiedler, A. T.; Halfen, H. L.; Brunold, T. C.; Halfen, J. A. *J. Am. Chem. Soc.* **2004**, *126*, 7627.

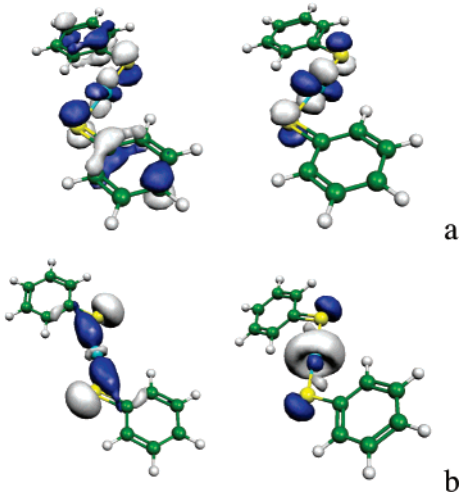

Figure 6. a: Bonding and antibonding d_{yz}/π_{op} interaction in the Fe-thiolate model complex. b: Bonding (Mn complex) and antibonding (Ni complex) d_{z^2}/π_{ip} interaction.

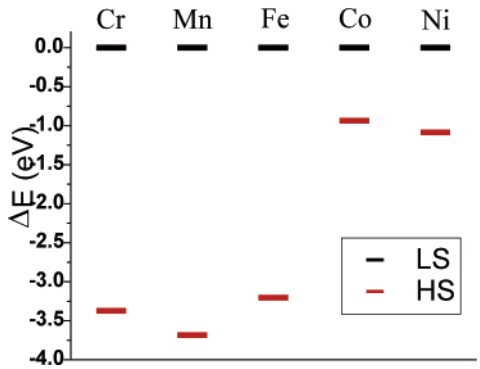

Figure 7. The calculated adiabatic high-spin/low-spin energy differences in the model complexes $M(SPh)_2$ (M = Cr−Ni).

are the lowest in energy (they lie below π_{ip} and π_{op}), in the Ni complex only d_{xy} lies above the π_{op} and for Zn, where all the d orbitals (not shown in the Figure 5) lie almost 5 eV below the π_{ip} and π_{op} thiolate orbitals. The analysis of the MO composition for different complexes also provides some useful information. The low-lying π_{ip} and π_{op} are pure thiolate orbitals, with no metal character, while the metal orbitals usually contain some of π_{ip} and π_{op} character.

Due to the linear or quasi linear geometries, a spatial overlap can easily occur between the pairs of the metal and ligand MO's. The strength of the interaction between ligand and metal orbital will depend on the M−S−C angle. The π_{ip} thiolate MO is mostly associated with a d_{z^2} metal orbital (Figure 6a), and to a lesser extent the d_{xz} orbital (e.g. in Cr and Co complexes) or with $d_{x^2-y^2}$ orbital (in the Ni complex). The π_{op} thiolate MO is uniquely associated with d_{yz} orbital. The bonding and antibonding interaction between d_{yz} and π_{op} MO's in the Fe complex are presented in Figure 6b. The calculation of the adiabatic high spin/low spin energy differences were performed on the high spin optimized geometries and yielded the values compiled in Figure 7. It is clear that these differences are qualitatively related to the difference in the number of the unpaired electrons in the low spin or high spin states. For Cr, Mn and Fe compounds, this difference is 3, 5 and 4 respectively, while it is 2 for the remaining Co and Ni species.

Conclusions. Six new monomeric, first row transition metal(II) thiolates have been prepared and characterized. They feature coordination by two sulfurs from the thiolate ligands as well as further interactions of varying strength from ipso carbons of flanking rings of the terphenyl ligands. These supplementary interactions are strongest for the chromium and iron derivatives and weakest for those of manganese and zinc. The iron dithiolate undergoes a unique bending of the metal coordination that was attributed to the tendency of the complex to attain an 18-electron configuration by interacting with the π-electrons of the aryl rings.

Acknowledgment. We are grateful to the donors of the Petroleum Research Fund administered by the American Chemical Society for financial support. M.B. thanks the Swiss National Science Foundation (Grant 8220-067593).

Supporting Information Available: X-ray crystallographic CIF files for compounds **1**−**6** and some details of DFT calculations. This material is available free of charge by the Internet at http://pubs.acs.org. See any current masthead page for ordering information and Web access instructions.

JA042958Q